Confocal versus interference microscopy - 3D resolution analysis

Yijian Zou[a], Tobias Pahl[a], Felix Rosenthal[a], and Peter Lehmann[a]

[a]Measurement Technology Group, Faculty of Electrical Engineering and Computer Science, University of Kassel, Wilhelmshöher Allee 71, 34109 Kassel, Germany

ABSTRACT

Confocal and interference microscopy are the two most widely used optical techniques for surface topography measurement. Nonetheless, due to diffraction effects, which are inevitable in optical far-field measurement methods, both techniques are limited in their lateral resolution. In contrast to conventional microscopes, where the lateral resolution is usually defined by a single number such as the Abbe limit, a more comprehensive (3D) characterization of resolution is required for surface topography measurement. The instrument transfer function (ITF) provides the height response of a profiler as a function of the surface's lateral spatial frequency content assuming linear systems theory. Comparing numerically calculated ITFs, we outline that interference microscopy can outperform confocal microscopy in terms of both, lateral and axial resolution, provided that appropriate signal processing is being used.

Keywords: confocal microscopy, coherence scanning interferometry, instrument transfer function, surface topography measurement, 3D resolution, white light interferometry, interference microscopy, Fourier optics

1. INTRODUCTION

Optical profilers operating in the measurement object's far-field are widely used for a fast and contactless inspection of surface textures. Interference[1–3] and confocal microscopy (CM)[4–6] are the most common optical measurement techniques for analyzing surface topographies with geometric features in the micro- and nanoscale. Similar to all optical profilers detecting scattered light in the object's far-field, confocal and interference microscopes are diffraction limited resulting in a lateral resolution in the range of hundreds of nanometers.

The lateral resolution of microscopes is usually defined by a single value such as the Abbe limit or Rayleigh criterion[7] assuming that the measurement object is placed in the focal plane of the microscope objective. For quantification, the imaging of gratings of certain period length or point scatterers, resulting in the so-called point-spread function (PSF), is considered. The minimum resolvable period length of a grating or the lateral width of the PSF provide a measure for the lateral resolution. Since the full width at half maximum (FWHM) of the PSF for confocal microscopes is theoretically narrower than for conventional microscopes,[6,8,9] confocal microscopes are usually assumed to offer slightly improved lateral resolution.

With regard to axial resolution, interference microscopy detects phase information enabling a height resolution with repeatability in the subnanometer range,[2,3] which is in principle independent of the numerical aperture (NA) of the microscope objective. In contrast, the axial resolution of confocal microscopes depends on the width of the axial response curve, which is mainly due to the NA. The height resolution of confocal microscopes is typically in the order of a few nanometers assuming microscope objectives of high NA.[6]

However, with respect to surface topography measurements, a single value for lateral or axial resolution is not sufficient, since the detected surface height response depending on the feature size plays a crucial role. To overcome this issue, the so-called instrument transfer function (ITF), which describes the measured amplitude of a sinusoidal surface depending on the spatial frequency, is currently used.[10–13]

In this study we compare numerically calculated ITF curves for confocal and interference microscopes. Representative for interference microscopy, coherence scanning interferometry (CSI), also referred to as white light interferometry (WLI), is considered as one of the most commonly used techniques.[3] Simulations are performed

Further author information: (Send correspondence to Tobias Pahl)
Tobias Pahl: E-mail: tobias.pahl@uni-kassel.de

Uni Kassel, FB16, FG Messtechnik

Author copy. Copyright 2025, Society of Photo-Optical Instrumentation Engineers (SPIE), see last page for details.

with the so-called universal Fourier optics (UFO) model, which can be applied to CSI[14] as well as confocal microscopy.[15] The UFO model provides fast simulation results of the measurement process assuming that the measurement object's surface fulfills the limitations of the Kirchhoff approximation of physical optics as described by Beckmann and Spizzichino.[16] However, since the ITF is usually defined based on sinusoidal surfaces of small amplitude, the assumptions of the Kirchhoff approximation are satisfied. Thus, rigorous models published in previous studies[17–19] are not considered for computational reasons. It should be noted that the UFO model provides similar results as the so-called Kirchhoff pupil integration model[20] and the foil-model[21] as shown elsewhere.[22,23] In addition, the UFO model is similar to the elementary Fourier optics model,[24,25] but more general since the measurement process is described in terms of a three-dimensional (3D) transfer function (TF) instead of the two-dimensional (2D) modulation transfer function (MTF).

Previous studies demonstrated that the signal processing algorithm used to reconstruct the surface height from measured image stacks and the fringe frequency, at which the phase of the image stack is analyzed, significantly affect the lateral resolution and the surface height obtained by CSI instruments.[26–28] Using an adapted signal processing strategy, we outline that CSI outperforms confocal microscopy with respect to 3D resolution.

2. MODEL AND SIGNAL PROCESSING

The 3D transfer function, which describes the measurement process of CSI as well as CM in the 3D spatial frequency domain (**q**-space), builds the basis of the UFO model. Figure 1(a) displays a cross-section of the 3D TF in the $q_x q_z$-plane for a microscopic setup of NA = 0.9 and monochromatic light of wavelength $\lambda = 440\,\text{nm}$. The equations used to calculate the 3D TF are derived in a previous publication.[29] It should be noted that the 3D TF refers to the electric field and not to the intensity. However, as outlined elsewhere,[20] both, the measurement processes of CSI and CM, can be modeled by integration of the electric field components and thus are mathematically well represented by the given transfer function. A general description of the setups considered and their modeling is published by Pahl et al.[20]

Image stacks, which correspond to a set of images captured by a camera at different axial positions of the measurement object, can be described in the 3D spacial frequency domain by the product

$$\tilde{I}(\mathbf{q}) = H(\mathbf{q})u_\mathrm{s}(\mathbf{q}) \tag{1}$$

of the 3D transfer function $H(\mathbf{q})$ and the scattered field $u_\mathrm{s}(\mathbf{q})$. According to the phase object approximation,[16] the scattered field can be written in terms of

$$u_\mathrm{s}(\mathbf{q}) = \mathcal{F}_{xy}\{\mathrm{e}^{-\mathrm{i}q_z h(x,y)}\}, \tag{2}$$

where $\mathbf{q} = (q_x, q_y, q_z) = \mathbf{k}_\mathrm{s} - \mathbf{k}_\mathrm{in}$ is the spatial frequency vector with the scattered and incident wave vectors $\mathbf{k}_\mathrm{s}$ and $\mathbf{k}^\mathrm{in}$, $h(x, y)$ represents the surface height function and $\mathcal{F}_{xy}$ denotes the 2D Fourier transform in the lateral x and y directions.[14] Figures 1(b) and 1(c) show $\tilde{I}(\mathbf{q})$ considering the transfer function displayed in Fig. 1(a) and a sinusoidal surface height function with a peak-to-valley (PV) amplitude of 25 nm and a period length of $L_x = 2.5\,\mu\text{m}$ (Fig. 1(b)) or L_x =400 nm (Fig. 1(c)). Due to the periodicity of the grating, diffraction orders appear at discrete positions $q_{x,n} = 2\pi n/L_x$. As a consequence, more diffraction orders occur at smaller lateral spatial frequencies for $L_x = 2.5\,\mu\text{m}$ compared to the grating of $L_x = 400\,\text{nm}$, where only the 0th and $\pm$1st order of diffraction are within the limits of the 3D TF. With respect to the shape of the 3D TF (see Fig. 1(a)), the axial spatial frequencies, at which the diffraction orders are visible, differ depending on the lateral spatial frequency component. This effect plays a crucial role for the choice of appropriate signal processing parameters as demonstrated later in this section.

Note that in the case of confocal microscopy, the measured intensity is not proportional to the strength of the scattered electric field. Hence, Eq. (1) is only valid for CSI. With respect to CM, the electric field in the spatial frequency domain is represented by the field distribution

$$u_\mathrm{meas}(\mathbf{q}) = H(\mathbf{q})u_\mathrm{s}(\mathbf{q}). \tag{3}$$

The field captured in the image plane follows from the inverse 3D Fourier transform and the intensity is obtained by $I_\mathrm{meas}(\mathbf{r}) \sim |u_\mathrm{meas}(\mathbf{r})|^2$, where $\mathbf{r}$ represents the lateral coordinates and the focus position z of the object. For

Uni Kassel, FB16, FG Messtechnik

Author copy. Copyright 2025, Society of Photo-Optical Instrumentation Engineers (SPIE), see last page for details.

more information on the UFO model for CM, we refer to Rosenthal et al.[15]
In order to reconstruct the surface topography from CSI image stacks, the envelope of an interference signal is analyzed to avoid ambiguities. For higher precision phase analysis is performed.[14,30] The maximum intensity and the corresponding axial position of the envelope is determined using a Gaussian fitting algorithm for each camera pixel. The phase is obtained for each pixel of the image stack at a certain axial spatial frequency $q_{z,\mathrm{eval}}$ also referred to as fringe or evaluation frequency. Figure 1(d) displays cross-sections from Fig. 1(a) at certain q_z positions marked by horizontal lines of the same color. The cross-sections demonstrate that the transfer behavior significantly depends on the axial spatial frequency, which can be accessed by the choice of $q_{z,\mathrm{eval}}$. The blue line corresponds to the axial position of maximum bandwidth. The red line is extracted from a higher spatial frequency and has a smaller bandwidth. Note that adjusting the axial spatial frequency in CSI signal processing is not state-of-the-art. Instead, CSI image stacks are typically analyzed at a so-called equivalent frequency (or analoguously equivalent wavelength), which is determined from analytical considerations or calibration measurements.[24,25,31] This equivalent wavelength generally lies somewhere at higher q_z positions compared to the blue line, and hence the bandwidth is worse. The green line is extracted for a small fringe frequency, which is below the blue line. In this case, the bandwidth is again worse and the transfer function does not act as a low-pass filter, but as a band-pass filter. However, the maximum detectable lateral frequency is increased compared to the blue line. Therefore, if for instance gratings of small period length are to be measured (see e.g. Fig. 1(c)), the image stack should be analyzed at small fringe frequencies to achieve the best lateral resolution. Figure 1(e) shows reconstructed sinusoidal gratings for two different evaluation frequencies. The nominal grating with PV amplitude of 25 nm and $L_x = 400\,\mathrm{nm}$ is plotted in blue. As demonstrated, the amplitude of the reconstructed profiles is reduced for both fringe frequencies. However, the height differs depending on the fringe frequency. Thus, the fringe frequency is adjusted depending on the period length in order to obtain the best topography fidelity[10] in this paper. It should be mentioned that especially for small amplitudes the scattered field (see Eq. (2)) is approximately proportional to the surface height.[27] As a consequence, the reconstructed amplitudes can be related to the values of the transfer function at the specific evaluation frequency. Figure 1(f) displays a cross-section of a 3D TF in $q_x q_z$-plane for NA = 0.9, but in this case for a broadband light source of central wavelength $\lambda_c = 440\,\mathrm{nm}$ and full width at half maximum (FWHM) of 80 nm. The spectral distribution is assumed to be a Gaussian function as described in Ref.[14] Due to the spectral width of the light source, the high lateral spatial frequency components of the transfer function are blurred. This observation is in agreement with a previous publication.[28] Therefore, we expect to obtain a lower amplitude from gratings with small period lengths using broadband compared to (nearly) monochromatic light sources.
In the case of confocal microscopes, the phase is not accessible. Instead, a narrower intensity curve is analyzed as a result of the depth response. The maximum intensity is then found by using a Gaussian fitting algorithm. More information on existing signal processing algorithms for confocal microscopes is provided by Hagemeier et al.[32] With respect to broadband light sources, the spectrum of the light source cannot be considered in one 3D TF as done for CSI and shown in Fig. 1(f). Instead, the intensity I_{meas} is calculated for several monochromatic wavelengths apparent in the spectrum and the total intensity is obtained by integration.

Uni-Kassel, FB16, FG Messtechnik

Author copy. Copyright 2025, Society of Photo-Optical Instrumentation Engineers (SPIE), see last page for details.

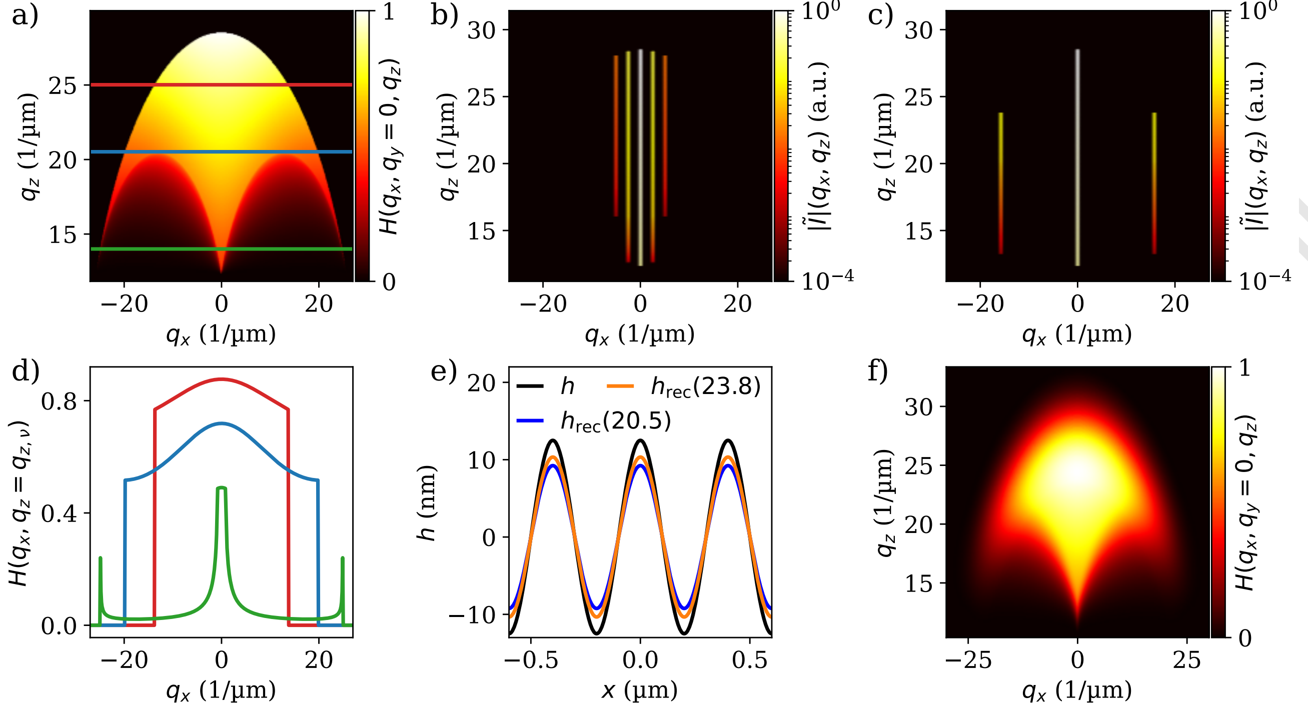

Figure 1. a) Cross-section of the 3D transfer function in $q_x q_z$-plane for NA = 0.9 and monochromatic light of $\lambda = 440\,\mathrm{nm}$; b), c) Fourier transformed CSI image stacks simulated for sinusoidal gratings with PV-amplitude of 25 nm and period length of 2.5 µm (b) and 400 nm (c); d) Line plots extracted from (a) at the positions of the lines of same color; e) Nominal (h) and reconstructed (h_{rec}) of sinusoidal grating from (c) with evaluation frequency of $q_{z,\mathrm{eval}} = 20.5\,\mathrm{µm}^{-1}$ and $q_{z,\mathrm{eval}} = 23.84\,\mathrm{µm}^{-1}$; f) Cross-section of the 3D transfer function in $q_x q_z$-plane for NA = 0.9 and broadband light of $\lambda_c = 440\,\mathrm{nm}$ and FWHM = 80 nm.

3. RESULTS

Using the simulation model introduced in Sec. 2, ITF curves are simulated and compared for CSI and CM considering monochromatic and polychromatic light sources. Since ISO standards[10] do not prescribe a specific amplitude, ITF curves are calculated for sinusoidal gratings with two different PV-amplitudes of 25 nm and 50 nm. The period lengths considered range from 100 nm to 10 µm yielding a spatial frequency range from $10\,\mathrm{µm}^{-1}$ to $0.1\,\mathrm{µm}^{-1}$. In addition, we assume a numerical aperture of 0.9, a perfectly reflective surface, and homogeneous illumination of the microscope objective's back focal plane for both measurement techniques. With CSI, the reconstruction of the surface topography is carried out by phase evaluation according to[14,30] as described in more detail in Sec. 2. Since the transmission behavior of the TF differs depending on q_z, see Fig. 1 (d), an optimally selected $q_{z,\mathrm{eval}}$ improves the results. In this context, a newly developed signal processing algorithm is applied in CSI, which performs the phase evaluation at an optimal $q_{z,\mathrm{eval}}$ value. The goal is to optimize the lateral resolution.

Figures 2(a) and 2(b) show ITF curves for CSI and CM with a PV-amplitude of 25 nm and 50 nm, respectively. In Fig. 2(a), the ITFs are simulated assuming monochromatic light of $\lambda = 440\,\mathrm{nm}$ for both measurement techniques. The results show that using CSI the ITF for spatial frequencies from $0.1\,\mathrm{µm}^{-1}$ to $1\,\mathrm{µm}^{-1}$ remains almost equal to 1 and shows a characteristic curve that is typical for CSI.[11] However, the ITF for CSI shows a minimal dependence on the height of the surface structure, which can be seen in the range of $1.5\,\mathrm{µm}^{-1}$, where a small step is visible for $h = 50\,\mathrm{nm}$. This dependence could be due to the signal processing algorithm and requires further investigation. It should be mentioned that a similar step is visible in experimental data published by de Groot.[11] For spatial frequencies of more than $4\,\mathrm{µm}^{-1}$ - which correspond to period lengths below 250 nm - the ITF drops rapidly. This can be attributed to the resolution limit of Abbe.[7]

In the case of CM, which works without a reference arm, the reconstruction is carried out by a Gaussian fitting

Uni Kassel, FB16, FG ... k

Author copy. Copyright 2025, Society of Photo-Optical Instrumentation Engineers (SPIE), see last page for details.

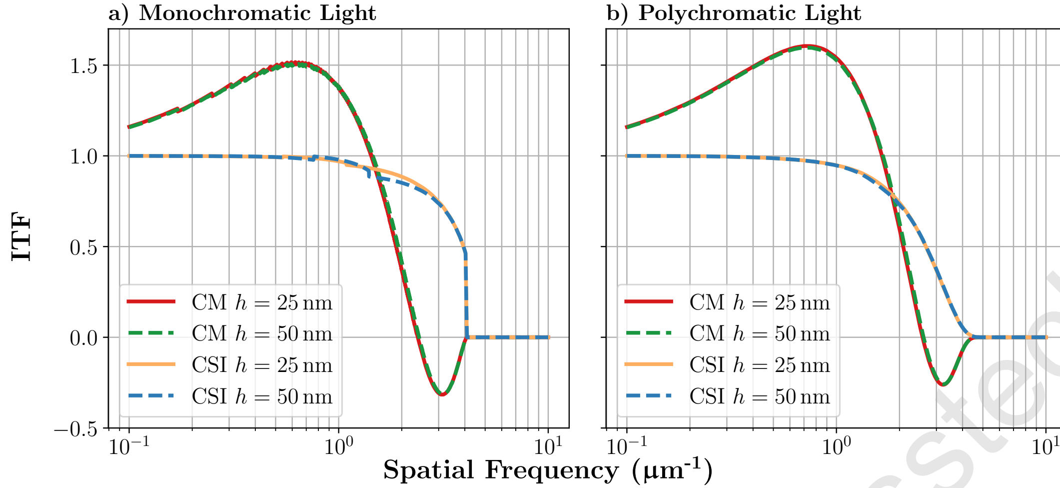

Figure 2. a) Simulated ITFs for CM and CSI with monochromatic illumination of wavelength $\lambda_c = 440\,\mathrm{nm}$; b) Simulated ITFs for CM and CSI with polychromatic illumination with a center wavelength of $\lambda_c = 440\,\mathrm{nm}$, FWHM $= 80\,\mathrm{nm}$ and a PV-amplitude of 25 nm and 50 nm. For CSI, the reconstruction of the input structure is performed for values of $q_{z,\mathrm{eval}}$, for which an optimum topography fidelity is achieved. In case of CM, a Gaussian fitting algorithm is used to reconstruct the height profiles from the image stack.

algorithm used to determine the maximum of the axial intensity curve for each pixel in the image stack as outlined by Hagemeier et al.[32] The ITF for CM is shown in Fig. 2(a) for both PV-amplitudes. The ITFs for different heights are approximately congruent, but both ITFs exhibit slight jumps. These can be explained by the use of monochromatic illumination, because the 3D transfer function has a clearly defined geometry with sharp boundaries for monochromatic illumination. In combination with the discretization in **q**-space, steps arise at the arc of the 3D TF.[27,28] These in turn lead to a varying rise and fall in the simulated ITF, as shown in Fig. 2(a). Using polychromatic illumination, the 3D TF for CSI becomes blurred with increasing FWHM as demonstrated in Fig. 1(f). This effect has already been investigated by Lehmann et al.[28] In the case of CM, intensities obtained for different wavelengths superimpose. As a result, the ITF curves for CSI and CM in Figure 2(b), which are obtained assuming a broadband light source of FWHM $= 80\,\mathrm{nm}$, become clearly more smooth.

The differences are particularly noticeable at spatial frequencies greater than $1.5\,\mu\mathrm{m}^{-1}$. In this range, the ITF for CM decreases almost linearly and reaches zero crossing at $2.4\,\mu\mathrm{m}^{-1}$. After this zero crossing, the phase of the reconstructed profile is inverted and the ITF reaches a minimum at $3.1\,\mu\mathrm{m}^{-1}$ with a ratio of -0.316 between the reconstructed and nominal surface amplitude. The ITF then rises to zero again due to the fundamental resolution limit.

A similar behavior of the ITF can be observed for CSI, if the height reconstruction is based on the position of the maximum of the envelope. The dashed blue line in Fig. 3(a) displays the ITF of CSI obtained using envelope evaluation. The dashed green line, representing the ITF for CM corresponds to the dashed green line in Fig. 2(a). This type of signal processing can lead to an inversion of the height values of the reconstructed profile for CSI with small period lengths, as already shown by Lehmann et al.[28] Since the signal processing applied to CSI and CM image stacks are similar (for envelope evaluation in case of CSI) and in Fig. 3(a) the ITFs even appear congruent, we assume that the inversion of the reconstructed profile in CM is subject to the same causes as in CSI. With regard to larger period length, the amplitude is overestimated by a factor up to 1.5 for both, CM and CSI with envelope analysis. Such an overestimation has already been observed in previous studies especially for CSI[17] and is explained by Lehmann et al.[28] Due to similar microscopic transfer characteristics of CM and CSI, the explanation probably holds for CM as well.

Figure 3(b) shows the ITF for CSI and CM for polychromatic illumination of $\lambda_c = 440\,\mathrm{nm}$ and FWHM $= 80\,\mathrm{nm}$. Note that no significant differences are obtained between PV-amplitudes of 25 nm and 50 nm as already shown in Fig. 2. Thus, Fig. 2(b) displays results for 50 nm only. However, the ITF of CSI and CM show minimal

Uni Kassel, FB16, FG Messtechnik

Author copy. Copyright 2025, Society of Photo-Optical Instrumentation Engineers (SPIE), see last page for details.

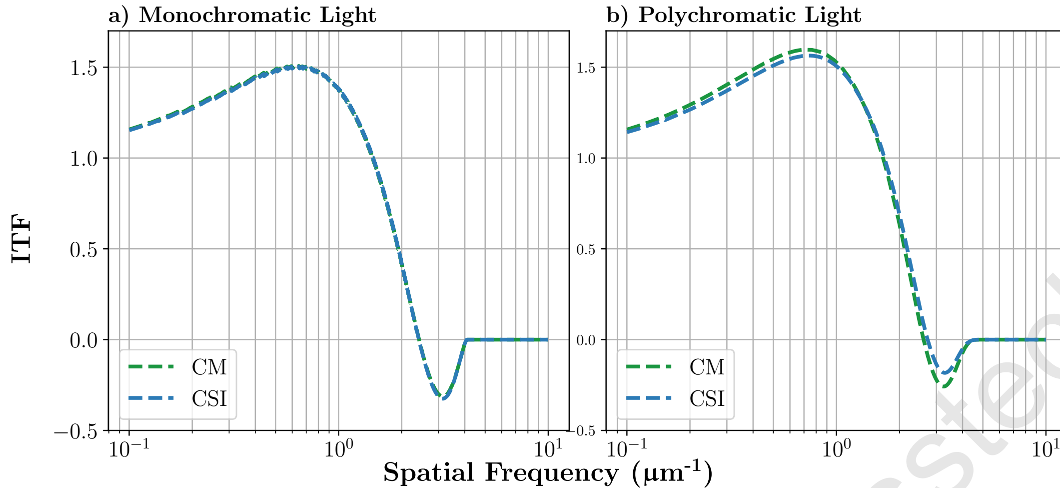

Figure 3. a) Simulated ITFs for CM and CSI with monochromatic light of 440 nm and a PV-amplitude of 50 nm; b) Simulated ITF for CM and CSI with polychromatic light with center wavelength λ_c = 440 nm, FWHM = 80 nm and a PV-amplitude of 50 nm. For CSI and CM a Gaussian fit algorithm is used to reconstruct the topography data for each pixel of the image stack. For better comparability, the same CM curves as shown in Fig. 2 (a) and (b) are presented here again.

differences in contrast to monochromatic illumination. Especially in the inversion area, the ITF value is larger for CSI with -0.185 than for CM with - 0.26. If the absolute values in the inversion area are considered, CM shows a slightly better lateral resolution, although the same signal processing algorithm is used.
In sum, the ITF for CSI under consideration of phase analysis yields an improved lateral resolution compared to CM. Confocal microscopy suffers from overestimation for larger period length, a zero-crossing and spatial frequency range, where the measured profile is inverted. Especially, the zero-crossing, where the amplitude of the measured profile is zero for a certain period length, and the range of inversion reduce the accuracy of confocal microscopes significantly, when surface topographies with features of small geometric extent are to be measured. Similar results are obtained for CSI if the profile reconstruction is solely based on envelope analysis. Comparing CM and CSI envelope results, CM shows a slightly improved resolution for small period length, which is in agreement with previous results comparing confocal with conventional microscopes.[6,8,9]

4. CONCLUSION

The instrument transfer function is simulated for confocal microscopy and coherence scanning interferometry (CSI) to compare both measurement techniques with respect to 3D resolution. The simulation model uses the phase object approximation and is fast as well as accurate as validated in previous publications.[22,23] In order to achieve the optimal 3D resolution for coherence scanning interferometers, the signal processing is adjusted appropriately. The calculated ITF curves demonstrate that CSI provides more accurate results compared to confocal microscopy if phase analysis is used. In contrast, results obtained by confocal microscopy are similar and only slightly better compared to those obtained by CSI envelope analysis. In general, the detected amplitude is overestimated for longer period lengths and the topography is inverted for shorter period lengths. In addition, a zero-crossing appears for a certain frequency between the overestimation and the inversion ranges, which significantly disturbs measurements for specific period lengths. Hence, care must be taken to analyzing the results of confocal microscopy and CSI with envelope evaluation for surface periods, which are close to the lateral resolution limit. In sum, we demonstrated that CSI provides better results analyzing measurement objects with surface features close to the lateral resolution limit if appropriate signal processing is used.
Since the results presented are solely based on numerical calculations, experimental validation is planned for future studies. Effects such as inversion and overestimation have already been demonstrated and explained

Uni Kassel, FB16, FG Messtechnik

Author copy. Copyright 2025, Society of Photo-Optical Instrumentation Engineers (SPIE), see last page for details.

for CSI, but not yet for confocal microscopes. In addition, the signal processing and the adjustment of the corresponding parameters such as the fringe frequency at which CSI signals are analyzed, can be subject to further improvement aiming at a fully automated signal processing, for instance.

ACKNOWLEDGMENTS

The authors gratefully acknowledge the financial support of the following research projects (GZ: LE 992/14-3 and LE 992/18-1) by the Deutsche Forschungsgemeinschaft (DFG).

REFERENCES

[1] Schmit, J., Creath, K., and Wyant, J., "Surface profilers, multiple wavelength, and white light interferometry," in [*Optical Shop Testing*], Malacara, D., ed., 667–755, Wiley, Ney York (2007).

[2] de Groot, P., "Phase shifting interferometry," in [*Optical Measurement of Surface Topography*], Leach, R., ed., 167–186, Springer, Berlin Heidelberg (2011).

[3] de Groot, P., "Coherence scanning interferometry," in [*Optical Measurement of Surface Topography*], Leach, R., ed., 187–208, Springer, Berlin Heidelberg (2011).

[4] Wilson, T., [*Confocal Microscopy*], Academic Press, London (1990).

[5] Corle, T. R. and Kino, G. S., [*Confocal Scanning Optical Microscopy and Related Imaging Systems*], Academic Press, San Diego (1996).

[6] Artigas, R., "Imaging confocal microscopy," in [*Optical Measurement of Surface Topography*], Leach, R., ed., 237–286, Springer, Berlin Heidelberg (2011).

[7] Singer, W., Totzeck, M., and Gross, H., [*Handbook of optical systems, volume 2: Physical image formation*], John Wiley & Sons, Weinheim (2006).

[8] Sheppard, C. J., "Scanning confocal microscopy," in [*Encyclopedia of Optical Engineering*], Hoffman, C. and Driggers, R., eds., 2525–2544, CRC Press, Boca Raton (2003).

[9] Kim, C.-S. and Yoo, H., "Three-dimensional confocal reflectance microscopy for surface metrology," *Measurement Science and Technology* **32**(10), 102002 (2021).

[10] "ISO 25178-600 Geometrical product specifications (GPS)—Surface texture: Areal—Part 600: Metrological characteristics for areal-topography measuring methods," (2019).

[11] de Groot, P. J., "The instrument transfer function for optical measurements of surface topography," *Journal of Physics: Photonics* **3**(2), 024004 (2021).

[12] de Groot, P. J., Daouda, Z., Deck, L. L., and Colonna de Lega, X., "Linear systems characterization of the topographical spatial resolution of optical instruments," *Applied Optics* **63**(15), 4201–4210 (2024).

[13] de Groot, P., Kramer, J., and Sutherland, T., "Modeling the topographic lateral resolution of interferometers," *Proc. SPIE* **12619**, 126190N (2023).

[14] Lehmann, P., Pahl, T., and Riebeling, J., "Universal Fourier optics model for virtual coherence scanning interferometers," *Proc. SPIE* **12619**, 126190O (2023).

[15] Rosenthal, F., Pahl, T., Eckhardt, T., Hagemeier, S., Compagnone, J., Czasch, T., Diehl, M., Koops, R., and Lehmann, P., "Universal Fourier optics model for virtual confocal microscopes," *Proc. SPIE* **12997**, 129970N (2024).

[16] Beckmann, P. and Spizzichino, A., [*The scattering of electromagnetic waves from rough surfaces*], Artech House, Inc., Norwood (1987).

[17] Pahl, T., Hagemeier, S., Künne, M., Yang, D., and Lehmann, P., "3D modeling of coherence scanning interferometry on 2D surfaces using FEM," *Optics Express* **28**(26), 39807–39826 (2020).

[18] Pahl, T., Hagemeier, S., Bischoff, J., Manske, E., and Lehmann, P., "Rigorous 3D modeling of confocal microscopy on 2D surface topographies," *Measurement Science and Technology* **32**(9), 094010 (2021).

[19] Pahl, T., Rosenthal, F., Künne, M., Käkel, E., Hagemeier, S., Diehl, M., Hillmer, H., and Lehmann, P., "Rigorous full 3D modeling of coherence scanning interferometry and confocal microscopy," *Journal of Physics: Photonics* (2025).

Uni Kassel, FB16, FG Messtechnik

Author copy. Copyright 2025, Society of Photo-Optical Instrumentation Engineers (SPIE), see last page for details.

[20] Pahl, T., Rosenthal, F., Breidenbach, J., Danzglock, C., Hagemeier, S., Xu, X., Künne, M., and Lehmann, P., "Electromagnetic modeling of interference, confocal, and focus variation microscopy," *Advanced Photonics Nexus* **3**(1), 016013–016013 (2024).

[21] Su, R. and Leach, R., "Physics-based virtual coherence scanning interferometer for surface measurement," *Light: Advanced Manufacturing* **2**(2), 120–135 (2021).

[22] Hooshmand, H., Pahl, T., de Groot, P. J., Lehmann, P., Pappas, A., Su, R., Leach, R., and Piano, S., "Comparison of Fourier optics-based methods for modeling coherence scanning interferometry," *Optical Engineering* **63**(4), 044102–044102 (2024).

[23] Czasch, T., Pahl, T., Rosenthal, F., Künne, M., and Lehmann, P., "Extension of the 3D analytical transfer function for coherence scanning interferometry," *Measurement* , 117617 (2025).

[24] de Groot, P. J. and Colonna de Lega, X., "Fourier optics modeling of interference microscopes," *Journal of the Optical Society of America A* **37**(9), B1–B10 (2020).

[25] de Groot, P., Colonna de Lega, X., Su, R., Coupland, J., and Leach, R., "Modeling of coherence scanning interferometry using classical Fourier optics," *Optical Engineering* **60**(10), 104106–104106 (2021).

[26] Lehmann, P., Xie, W., Allendorf, B., and Tereschenko, S., "Coherence scanning and phase imaging optical interference microscopy at the lateral resolution limit," *Optics Express* **26**(6), 7376–7389 (2018).

[27] Lehmann, P., Künne, M., and Pahl, T., "Analysis of interference microscopy in the spatial frequency domain," *Journal of Physics: Photonics* **3**(1), 014006 (2021).

[28] Lehmann, P., Hagemeier, S., and Pahl, T., "Three-dimensional transfer functions of interference microscopes," *Metrology* **1**(2), 122–141 (2021).

[29] Lehmann, P. and Pahl, T., "Three-dimensional transfer function of optical microscopes in reflection mode," *Journal of Microscopy* **284**(1), 45–55 (2021).

[30] Tereschenko, S., *Digitale Analyse periodischer und transienter Messsignale anhand von Beispielen aus der optischen Präzisionsmesstechnik*, PhD thesis, University of Kassel (2018).

[31] Sheppard, C. J. and Larkin, K. G., "Effect of numerical aperture on interference fringe spacing," *Applied Optics* **34**(22), 4731–4734 (1995).

[32] Hagemeier, S., Pahl, T., Breidenbach, J., and Lehmann, P., "A novel cubic-exp evaluation algorithm considering non-symmetrical axial response signals of confocal microscopes," *Microscopy Research and Technique* **86**(8), 1012–1022 (2023).

Uni-Kassel, FB16, FG Messtechnik

Y. Zou, T. Pahl, F. Rosenthal, P. Lehmann, "Confocal versus interference microscopy: 3D resolution analysis" EPJ Proc. SPIE 13567, Optical Measurement Systems for Industrial Inspection XIV, 135670Y (2025)

https://doi.org/10.1117/12.3060501

Copyright 2025, Society of Photo-Optical Instrumentation Engineers (SPIE). One print or electronic copy may be made for personal use only. Systematic reproduction and distribution, duplication of any material in this paper for a fee or for commercial purposes, or modification of the content of the paper are prohibited.